

# PhysConvex: Physics-Informed 3D Dynamic Convex Radiance Fields for Reconstruction and Simulation

Dan Wang<sup>1</sup> Xinrui Cui<sup>2</sup> Serge Belongie<sup>3</sup> Ravi Ramamoorthi<sup>1</sup>

<sup>1</sup>University of California, San Diego <sup>2</sup>University of North Texas <sup>3</sup>Copenhagen University

{danwang, ravir}@ucsd.edu, xinrui.cui@unt.edu, s.belongie@di.ku.dk

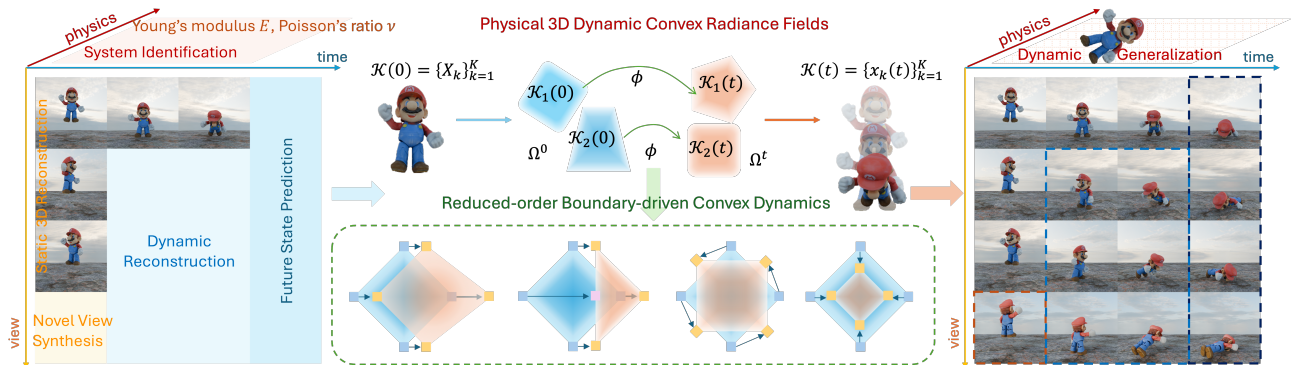


Figure 1. PhysConvex introduces boundary-driven dynamic convex fields integrated with reduced-order convex simulation for unified 3D reconstruction and dynamics. It recovers appearance, geometry, and physics from multi-view videos, enabling mesh-free, physically consistent, visually realistic simulation.

## Abstract

Reconstructing and simulating dynamic 3D scenes with both visual realism and physical consistency remains a fundamental challenge. Existing neural representations, such as NeRFs and 3DGS, excel in appearance reconstruction but struggle to capture complex material deformation and dynamics. We propose PhysConvex, a Physics-informed 3D Dynamic Convex Radiance Field that unifies visual rendering and physical simulation. PhysConvex represents deformable radiance fields using physically grounded convex primitives governed by continuum mechanics. We introduce a boundary-driven dynamic convex representation that models deformation through vertex and surface dynamics, capturing spatially adaptive, non-uniform deformation, and evolving boundaries. To efficiently simulate complex geometries and heterogeneous materials, we further develop a reduced-order convex simulation that advects dynamic convex fields using neural skinning eigenmodes as shape- and material-aware deformation bases with time-varying reduced DOFs under Newtonian dynamics. Convex dynamics also offers compact, gap-free volumetric coverage, enhancing both geometric efficiency and simulation fidelity. Experiments demonstrate that PhysConvex achieves high-

quality reconstruction of geometry, appearance, and physical properties from videos, outperforming existing methods.

## 1. Introduction

Reconstructing the appearance, geometry, and physical properties of objects directly from visual observations is a fundamental yet challenging goal in computer vision. Traditional physics-based simulation methods [3, 14, 27, 38, 50] typically rely on the known geometry, limiting their applicability to real-world scenarios. Alternatively, purely neural approaches [6, 16–18, 29, 30, 35–37, 41, 44, 47, 48] directly model dynamics via learned networks from data. While effective for rendering, these approaches tightly couple extrinsic geometric attributes with intrinsic physical motion, disregarding underlying physical laws and thereby limiting generalization and interpretability.

Recent advances [9, 23, 28, 45, 51] have sought to bridge this gap by integrating radiance field representations, such as NeRF [32, 39] and Gaussians [24, 44, 46, 48], with differentiable physical simulators. These physics-informed frameworks jointly optimize geometry, appearance, and physical parameters, offering a unified approach to reconstruction and simulation. However, existing dynamic primitives (e.g., voxels in NeRF [28], ellipsoids in 3DGS [7, 9,

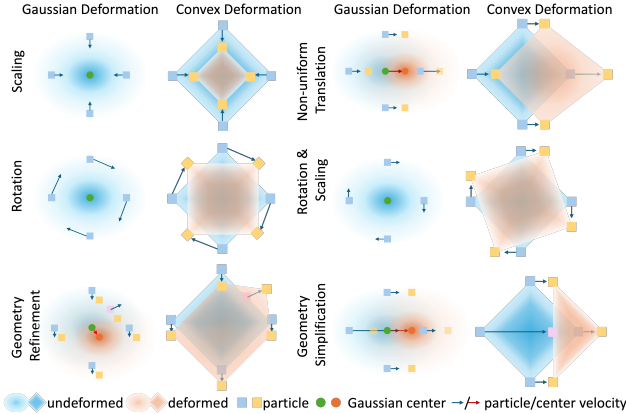


Figure 2. Center-driven Gaussian dynamics have limited flexibility for non-uniform deformation and evolving boundaries, while boundary-driven convex dynamics enable spatially adaptive vertex advection, explicit surface evolution, and polyhedral structural refinement.

51]) are primarily designed for rendering efficiency rather than physically consistent deformation, leading to several limitations (Fig. 2): First, in hybrid Eulerian-Lagrangian frameworks, center-driven dynamics update primitives using central particles or pooled neighbors, lacking spatial sensitivity to non-uniform deformation. Second, predefined particle-primitive bindings neglect material and geometric variation, resulting in inaccurate coupling. Third, mesh-free approaches using grid-based MPM simulation [22] with NeRFs and Gaussians struggle to represent sharp or evolving boundaries, hindering physically meaningful surface deformation. Finally, fixed ellipsoidal kernels, constrained by splatting efficiency, limit anisotropic or nonlinear material modeling and produce poor spatial coverage near planar or angular regions. In essence, rendering and simulation demand different properties on dynamic 3D primitives: compact appearance encoding versus geometric and physical expressiveness, which existing methods fail to reconcile.

To tackle these challenges, we propose **Physics-informed 3D dynamic Convex radiance fields** (PhysConvex), a unified framework for visual rendering and physical simulation (Fig. 1). PhysConvex represents deformable radiance fields using 3D dynamic convexes governed by continuum mechanics, extending static 3D convex primitives [19] to dynamic, physically consistent scenarios.

We introduce a **boundary-driven dynamic convex representation** (Sec. 4.1) that enables flexible, spatially adaptive, and physically consistent deformation (Fig. 2). We represent convex boundary deformation explicitly as vertex dynamics of convex hulls, or implicitly as the surface dynamics of half-space support functions. (a) *Vertex dynamics* advect individual convex vertices under Newtonian motion, providing spatial sensitivity and flexibility to non-uniform deformation; (b) *Surface dynamics* capture evolving edges and boundaries, allowing physically meaningful surface de-

formation; (c) *Convex dynamics* enable polyhedral structural modification, refinement, and simplification, enhancing geometric expressiveness and adaptability for simulating anisotropic materials. Moreover, deformable convexes approximate complex dynamic geometries with a compact set of primitives, achieving dense volumetric coverage and efficient, high-fidelity physical simulation.

To integrate convex primitives into physics-based dynamics, we develop a **reduced-order convex simulation** (Sec. 4.2) that captures rich deformation behaviors of complex geometries and heterogeneous materials without explicit meshes/grids or predefined bindings. Dynamic convex fields are advected under continuum mechanics, using spatially varying neural skinning eigenmodes as a physics-informed, shape- and material-aware deformation basis, with time-varying reduced degrees of freedom under Newtonian dynamics [33]. Finally, appearance, geometry, and physical parameters are jointly optimized through *differentiable simulation and rendering* (Sec. 4.3). In summary, our main contributions are:

- We propose *PhysConvex* that integrates physical dynamics with deformable 3D convex radiance fields for video-based reconstruction and simulation.
- We introduce a *boundary-driven dynamic convex representation* that combines vertex-/surface-level flexibility for spatially adaptive and physical coherent deformation.
- We present a *reduced-order convex simulation* that advects dynamic convex fields via neural skinning eigenmodes as physics-informed deformation bases for shape- and material-aware dynamics.
- Extensive experiments demonstrate that PhysConvex achieves high accuracy and efficiency in recovering geometry, appearance, and physical properties from videos, outperforming existing methods.

## 2. Related Work

**Physics-Based Simulation.** Classical physics simulation relies on mesh-based finite element methods (FEM) [2, 5, 11, 38], which require explicit meshing and linear shape functions, making them inflexible for complex or evolving geometries. Mesh-free methods such as the Material Point Method (MPM) [21, 22, 25, 49] and Smoothed Particle Hydrodynamics (SPH) [13, 26, 34] alleviate meshing but still depend on background grids or neighborhood connectivity, limiting efficiency and stability for highly nonlinear dynamics. Recent efforts, such as Spring-Gauss [51] employ mass-spring systems for elastic behavior, but remain restricted in generalizing to diverse materials. Model Order Reduction (MOR) approaches [3, 8, 10, 33, 50] offer efficient, mesh-free alternatives by learning reduced-order subspaces that enable accurate, real-time simulation of complex deformations. Inspired by these advances, our method develops a reduced-order convex simulation model that integrates vertex- and surface-based dynamics with differen-

tiable MOR simulation and rendering for geometry, appearance, and physical properties.

### Video-based Physical Reconstruction and Simulation.

Integrating physical simulation with neural 3D reconstruction has gained traction in works [9, 23, 28, 45, 51], integrating mesh-free simulation with NeRF or 3D Gaussian Splatting. However, most existing frameworks rely on neural primitives, such as voxels in NeRF [28] or ellipsoids in 3D Gaussian Splatting [23, 45, 51], combined with physics-based simulation. However, these primitives are primarily optimized for efficient rendering rather than modeling physically consistent deformation, resulting in several key limitations: lack of spatial deformation flexibility within primitives; difficulty modeling sharp or evolving boundaries; restricted shape expressiveness due to fixed-shape Gaussian or voxel kernels; and inaccurate binding between Eulerian rendering primitives and Lagrangian dynamics particles. To address this gap, we introduce PhysConvex, a unified framework for visual rendering and physical simulation. Inspired by 3DCS [19], PhysConvex presents a physical dynamic convex representation to reconstruct and simulate radiance fields governed by continuum mechanics.

## 3. Preliminaries

**Continuum Mechanics.** Continuum mechanics describes the motion of deformable objects through a time-dependent deformation map  $\mathbf{x} = \phi(\mathbf{X}, t)$ , which maps material coordinates  $\mathbf{X}$  in the undeformed reference domain  $\Omega^0$  to world coordinates  $\mathbf{x}$  in the deformed configuration  $\Omega^t$  at time  $t$ . The evolution of  $\phi$  is governed by the conservation of mass and momentum:

$$\int_{\Omega^t} \rho(\mathbf{x}, t) \equiv \int_{\Omega^0} \rho(\phi^{-1}(\mathbf{x}, t), 0), \quad (1)$$

$$\rho(\mathbf{x}, t) \dot{\mathbf{v}}(\mathbf{x}, t) = \nabla \cdot \boldsymbol{\sigma}(\mathbf{x}, t) + \mathbf{f}^{\text{ext}},$$

where  $\rho(\mathbf{x}, t)$  is the density field,  $\dot{\mathbf{v}}(\mathbf{x}, t) = \frac{\partial^2 \phi}{\partial t^2}$  is the acceleration, and  $\mathbf{f}^{\text{ext}}$  denotes external forces. The internal force is given by the Cauchy stress tensor  $\boldsymbol{\sigma}(\mathbf{x}, t)$ , which encodes local deformation behavior. The Jacobian of the deformation map,  $\mathbf{F}(\mathbf{X}, t) = \nabla_{\mathbf{X}} \phi(\mathbf{X}, t)$ , is the deformation gradient, representing local stretch, rotation, and shear, and is central to elasticity. The constitutive model defines the relationship between  $\mathbf{F}$ , the strain energy density function  $\Psi(\mathbf{F})$ , and the stress tensor  $\boldsymbol{\sigma}$ , parameterized by physical parameters Young’s modulus  $E$  and Poisson’s ratio  $\nu$ .

**Model Order Reduction.** Model order reduction (MOR) provides a compact, mesh-free alternative with efficient numerical integration and accurate modeling of nonlinear deformation. In MOR, the deformation map is parameterized as  $\mathbf{x} = \phi(\mathbf{X}, \mathbf{z}(t))$ , where  $\mathbf{z}(t)$  is a time-varying low-dimensional vector of reduced degrees of freedom (DOFs).

Using implicit time integration, the simulation is formulated as an optimization problem:

$$\mathbf{z}_{t+1} = \arg \min_{\mathbf{z}} \frac{1}{2} \|\mathbf{z} - \tilde{\mathbf{z}}_t\|_{\mathbf{M}}^2 + \Delta t^2 \mathbf{E}_{\text{potential}}(\mathbf{z}), \quad (2)$$

where  $\mathbf{E}_{\text{potential}}(\mathbf{z})$  denotes the total potential energy of the simulated object from internal and external forces,  $\Delta t$  is the timestep,  $\tilde{\mathbf{z}}_t$  is the first-order predictor, and  $\|\cdot\|_{\mathbf{M}}^2$  is the mass-matrix-weighted norm.

**3D Convex Splatting.** 3D Convex Splatting (3DCS) [19] represents radiance fields using smooth convex primitives, offering greater geometric expressiveness than Gaussians and enabling efficient modeling of scenes with sharp edges and dense volumes using fewer elements. A 3D convex is defined as the convex hull of a point set  $\mathcal{K} = \{\mathbf{x}_k\}_{k=1}^K$ , where the points  $\{\mathbf{x}_k\}$  define the hull of the shape, but are not necessarily explicit polyhedral vertices. A convex radiance field consists of  $N$  convex polytopes  $\mathcal{C} = \{\mathcal{K}_n, \mathbf{c}_n, \sigma_n, \alpha_n, \beta_n\}_{n=1}^N$ , where  $\mathbf{c}_n$  and  $\sigma_n$  denote color and opacity, and  $\alpha_n$  and  $\beta_n$  control smoothness and sharpness, respectively. Here,  $\alpha$  governs the softness of vertices and edges, and  $\beta$  modulates the radiance transition from diffuse to dense regions.

## 4. Method

Given a set of posed multi-view videos of a dynamic scene, our goal is to jointly recover the appearance and geometric representation, and the underlying physical properties (e.g., Young’s modulus, Poisson’s ratio) of the dynamic object.

**Method Overview.** PhysConvex introduces boundary-driven dynamic convex radiance fields (Sec. 4.1) integrated with physical reduced-order convex simulation (Sec. 4.2) to achieve differentiable physically-consistent 3D reconstruction and dynamic modeling (Sec. 4.3). PhysConvex is trained by enforcing rendered pixels to match the observed video in two stages (Fig. 3): (1) An undeformed convex field is reconstructed over the first multi-view frame; (2) The reduced-order convex simulation advects our boundary-driven dynamic convex radiance field under continuum mechanics, and physical properties can be optimized through joint differential simulation and rendering using single-view video supervision.

### 4.1. Boundary-driven Dynamic Convex Fields

A dynamic object can be approximated as a collection of time-varying convex polytopes, forming a piecewise representation of dynamic geometry. By extending with an additional time variable  $t \in \mathbb{R}^+$ , we parameterize our dynamic convex radiance field as a set of time-dependent  $N$  convex polytopes (convexes):

$$\mathcal{C}(t) = \{\mathcal{K}_n(t), \mathbf{c}_n, \sigma_n, \alpha_n, \beta_n\}_{n=1}^N,$$

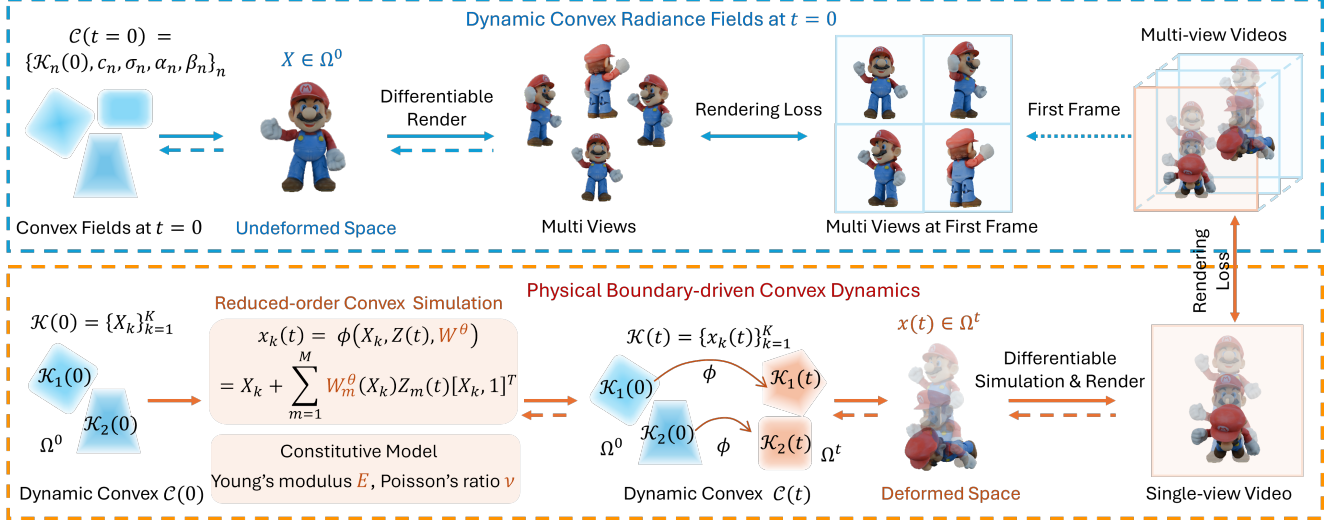


Figure 3. PhysConvex jointly reconstructs the geometry, appearance, and physical properties of dynamic objects by integrating boundary-driven dynamic convex field, differentiable reduced-order convex simulation, and rendering. Training proceeds in two stages: (1) reconstructing an undeformed convex field from the first multi-view frame, and (2) advecting the boundary-driven convex field via reduced-order simulation while jointly optimizing physical properties via differentiable simulation and rendering under single-view video supervision.

where  $\mathcal{K}_n(t)$  denotes the  $n$ -th dynamic convex at time  $t$ , and  $\{c_n, \sigma_n, \alpha_n, \beta_n\}$  are its time-invariant color, opacity, smoothness, and sharpness parameters.

We represent boundary-driven convex deformation explicitly as vertex dynamics of convex hulls, or implicitly as surface dynamics of half-space support functions, enabling spatially adaptive vertex deformation, physically meaningful surface evolution, and geometry modification through polyhedral structures (Fig. 2). Explicit vertex dynamics naturally support physical simulation, while implicit surface dynamics enable differentiable rendering.

## 4.2. Physical Reduced-order Convex Simulation

**Convex Vertex Dynamics.** A dynamic convex is defined as a 3D time-varying point set  $\mathcal{K}(t) = \{\mathbf{x}_k(t)\}_{k=1}^K$  representing the convex hull. During simulation, these points evolve under physical dynamics, enabling spatial flexibility and non-uniform shape deformation. The undeformed convex hull is denoted as  $\mathcal{K}(t=0) = \{\mathbf{X}_k\}_{k=1}^K$ .

To advect dynamic convex radiance fields, inspired by reduced-order simulation [33], we model the vertex dynamics  $\mathbf{x}_k(t)$  using spatially varying neural skinning eigenmodes  $W^\theta$  as reduced deformation bases,

$$\phi(\mathbf{X}_k, \mathbf{Z}(t), W^\theta) = \mathbf{X}_k + \sum_{m=1}^M W_m^\theta(\mathbf{X}_k) \mathbf{Z}_m(t) [\mathbf{X}_k, \mathbf{1}]^T, \quad (3)$$

where skinning eigenmodes  $W^\theta(\mathbf{X}) \in \mathbb{R}^3 \rightarrow \mathbb{R}^M$  represent physics-informed deformation bases encoding both shape and material awareness, and  $M$  is the number of reduced DOFs. The reduced bases  $W^\theta(\mathbf{X})$  are represented as a small MLP-based neural field parameterized by  $\theta$ , enabling smooth, mesh-free discretization for complex ge-

ometries and heterogeneous materials. The neural skinning field  $W^\theta(\mathbf{X})$  is trained to learn physically significant motions by minimizing deformation energy:

$$\begin{aligned} \theta^* = \arg \min_{\theta} & \lambda_{\text{elastic}} \int_{\mathbb{R}^3} \varphi(\mathbf{X}) \Psi(\phi(\mathbf{X}, \mathbf{z}, W^\theta)) \\ & + \lambda_{\text{ortho}} \sum_{i=1}^M \sum_{j=1}^M \int_{\mathbb{R}^3} \varphi(\mathbf{X}) (W_i^\theta W_j^\theta - \delta_{ij})^2 d\mathbf{X}, \end{aligned} \quad (4)$$

where  $\varphi(\mathbf{X})$  is a density function,  $\Psi(\cdot)$  is the strain energy density function, and  $\delta_{ij}$  is the Kronecker delta. This training encourages  $W^\theta(\mathbf{X})$  to encode low-dimensional, physically consistent deformation behaviors that are material- and shape-aware, achieving mesh-free model reduction.

$\mathbf{Z}(t) \in \mathbb{R}^{3 \times 4 \times M}$  represents time-varying reduced DOFs as handle transformation matrices, which are flattened into  $\mathbf{z}(t) = \text{flat}(\mathbf{Z}(t)) \in \mathbb{R}^{12 \times M}$ . During the simulation,  $\mathbf{z}(t)$  is initialized to zero to ensure that  $\mathbf{x}_k(0) = \mathbf{X}_k$ . At each discrete time step,  $\mathbf{z}(t)$  is updated via implicit time integration using the incremental potential formulation (Eq. 2) and solved through a standard Newton-based solver [4, 27]. This process advances the dynamic convex field under physically consistent reduced-order dynamics.

**Convex Surface Dynamics.** Given a dynamic convex point set, the convex hull can equivalently be expressed by  $H$  time-varying planes  $\mathcal{H}(t) = \{(\mathbf{n}_h(t), d_h(t))\}_{h=1}^H$ , where  $\mathbf{n}_h(t)$  and  $d_h(t)$  denote the normal and offset of the  $h$ -th plane, respectively. The signed distance of a point  $\mathbf{x}$  to the  $h$ -th time-dependent plane is defined as:

$$f_h(\mathbf{x}, t) = \mathbf{n}_h(t) \cdot \mathbf{x} + d_h(t). \quad (5)$$

Following the static indicator formulation in CvxNet [12], we define  $\mathcal{O}(\mathbf{x}, t) : \mathbb{R}^3 \rightarrow [0, 1]$  as the time-dependent occupancy function for each dynamic convex:

$$\begin{aligned} \mathcal{O}(\mathbf{x}, t) &= \text{Sigmoid}(-\beta \varphi(\mathbf{x}, t)), \\ \varphi(\mathbf{x}, t) &= \log \left( \sum_{h=1}^H \exp(\alpha f_h(\mathbf{x}, t)) \right), \end{aligned} \quad (6)$$

where  $\alpha$  and  $\beta$  control convex smoothness and sharpness, respectively, and  $\varphi(\mathbf{x}, t)$  approximates the signed distance function of a dynamic convex hull.

To render deformed convex kernels, we extend the splatting from 3DCS [19] to handle dynamic scenes. PhysConvex projects 3D time-varying points to 2D, constructs their dynamic convex hulls, and rasterizes them using  $\alpha$ -blending. Given camera pose and  $N$  dynamic convexes, the time-varying pixel color at location  $\mathbf{q}$  and time  $t$  is:

$$\mathbf{C}(\mathbf{q}, t) = \sum_{i=1}^N \mathbf{c}_i \sigma_i \mathcal{O}_i(\mathbf{q}, t) \prod_{j=1}^{i-1} (1 - \sigma_j \mathcal{O}_j(\mathbf{q}, t)), \quad (7)$$

where  $\mathbf{c}_i$  and  $\sigma_i$  denote the color and opacity of the  $i$ -th dynamic convex, respectively.

### 4.3. Differentiable Rendering and Simulation

Given posed multi-view videos of a dynamic scene, we reconstruct the dynamic object’s appearance, geometry, and physical properties through a joint differentiable simulation and rendering (Fig. 3).

**Appearance and Geometry Optimization.** To recover the undeformed convex radiance field  $\mathcal{C}(0)$ , we optimize from the first multi-view frames of the input videos by minimizing:

$$\begin{aligned} \mathcal{C}^*(0) &= \arg \min_{\{\mathcal{K}_n(0), \mathbf{c}_n, \sigma_n, \alpha_n, \beta_n\}} \mathcal{L}, \\ \mathcal{L} &= (1 - \lambda) \mathcal{L}_1 + \lambda \mathcal{L}_{\text{D-SSIM}} + \beta \mathcal{L}_m, \end{aligned} \quad (8)$$

where  $\mathcal{L}_1$  and  $\mathcal{L}_{\text{D-SSIM}}$  are image reconstruction losses, and  $\mathcal{L}_m$  regularizes the number of convexes following [19]. This optimization yields the undeformed convex radiance field  $\mathcal{C}^*(0) = \{\mathcal{K}_n^*(0), \mathbf{c}_n^*, \sigma_n^*, \alpha_n^*, \beta_n^*\}_{n=1}^N$  in material space  $\Omega^0$ .

**Physical Model Optimization.** To recover physical properties, we jointly optimize the elastic parameters  $\{E, \nu\}$  and the neural skinning field  $W^\theta$  with a single front-view video supervision:

$$\begin{aligned} E^*, \nu^*, \theta^* &= \arg \min_{E, \nu, \theta} \mathcal{L}_{\text{sim}}, \\ \mathcal{L}_{\text{sim}} &= \frac{1}{SP} \sum_{p=1}^P \sum_{s=1}^S \|\mathbf{C}(\mathbf{q}_p, t_s) - \mathbf{C}_{\text{gt}}(\mathbf{q}_p, t_s)\|_2^2, \end{aligned} \quad (9)$$

where  $\mathbf{C}$  and  $\mathbf{C}_{\text{gt}}$  denote the rendered and ground-truth pixel colors at each time step. Since both simulation and rendering are differentiable, physical and material parameters can be optimized end-to-end from video observations.

To equip our model with generalizable physical understanding, we adopt a feed-forward physical system identification framework inspired by [9]. Given a single front-view video, a pretrained video Vision Transformer [42] extracts motion cues and prior physical knowledge from large-scale video data. Small MLP regression heads then estimate  $\{E, \nu, \theta\}$ , providing an initial coarse prediction that is subsequently refined through differentiable simulation to better match reference videos. In summary, PhysConvex jointly reconstructs geometry, appearance, and physical properties of deformable objects by unifying physical boundary-driven dynamic convex representation, differentiable reduced-order convex simulation, and rendering.

## 5. Results

In this section, we evaluate PhysConvex on four tasks: physical system identification (Sec. 5.1), dynamic reconstruction (Sec. 5.2), future state prediction (Sec. 5.3), and physical generalization capability (Sec. 5.4).

**Baselines.** (1) **PAC-NeRF** [28] jointly reconstructed dynamic NeRFs and a simulatable model using MPM [22]. (2) **Spring-GS** [51] models elastic objects with spring-mass 3D Gaussians and learnable spring stiffness parameters, limited to elastic dynamics. (3) **GIC** [7] integrates 3D Gaussians with MPM simulation, enhancing shape reconstruction via a motion-factorized network and coarse-to-fine filling strategy. (4) **Vid2Sim** [9] is a feed-forward Gaussian-based model with reduced-order simulation by utilizing pretrained VideoMAE [42] and Large Multi-view Gaussian Model (LGM) [40] as backbones for reconstructing physical parameters and 3D Gaussians.

**Metrics.** For *physical parameters estimation*, we report Mean Absolute Error (MAE) of  $\log(E)$  and  $\nu$  under Neo-Hookean model (excluding Spring-GS). For *dynamic reconstruction and future prediction*, we measure PSNR[20], SSIM[43], and video perceptual loss (FoVVDP) [31].

**Dataset.** Following [9], we use 12 high-quality 3D meshes from Google Scanned Objects (GSO) [15], featuring complex geometries and detailed textures. Objects are simulated using FEM to obtain physically accurate reference dynamics. The animations are rendered from 12 viewpoints at a resolution of  $448 \times 448$  for 24 frames. The first 16 frames are used as observations, and the remaining 8 frames serve as ground-truth references for future state prediction.

**Physical Generalization Capability.** We test generalization to varied materials, novel force, and boundary conditions, demonstrating consistent performance (Sec. 5.4).

**Implementation details.** Each convex shape is initialized with  $K = 6$  points and spherical harmonics of de-

Table 1. Quantitative Comparison of Mean Absolute Error (MAE) on Physical System Identification.

	methods	backpack	bell	blocks	bus	cream	elephant	grandpa	leather	lion	mario	sofa	turtle	Mean Error ↓
$\log(E)$	PAC-NeRF	3.28	1.08	4.02	3.30	3.22	3.05	2.99	1.20	2.34	3.37	0.20	1.94	2.50
	GIC	1.16	2.87	2.12	1.93	2.13	1.53	<b>0.42</b>	3.45	2.85	1.82	0.65	3.18	2.01
	Vid2Sim	0.69	<b>0.15</b>	0.54	<b>0.26</b>	0.95	<b>0.18</b>	1.07	0.73	0.48	<b>0.50</b>	0.18	<b>0.44</b>	0.51
	<b>Ours</b>	<b>0.32</b>	0.34	<b>0.10</b>	0.28	<b>0.34</b>	0.60	0.97	<b>0.18</b>	<b>0.23</b>	0.54	<b>0.01</b>	0.56	<b>0.37</b>
$\nu$	PAC-NeRF	0.21	0.23	0.33	0.16	0.12	0.06	0.36	0.26	0.14	0.33	0.30	0.01	0.21
	GIC	0.11	0.24	0.29	0.18	0.08	0.24	0.26	<b>0.02</b>	0.14	0.22	<b>0.01</b>	0.08	0.16
	Vid2Sim	0.10	0.10	0.07	0.06	0.11	<b>0.05</b>	<b>0.02</b>	0.06	0.05	<b>0.06</b>	0.08	0.02	0.06
	<b>Ours</b>	<b>0.06</b>	<b>0.09</b>	<b>0.02</b>	<b>0.02</b>	<b>0.05</b>	0.08	0.03	<b>0.02</b>	<b>0.03</b>	0.12	0.02	<b>0.01</b>	<b>0.04</b>

Table 2. Quantitative Comparison on Dynamic Reconstruction.

		backpack	bell	blocks	bus	cream	elephant	grandpa	leather	lion	mario	sofa	turtle	Mean ↑
PSNR ↑	PAC-NeRF	19.37	25.00	23.36	20.72	23.24	22.27	21.63	20.85	22.66	21.01	22.49	22.19	22.06
	Spring-Gaus	17.42	20.49	22.78	20.06	23.58	21.30	21.64	18.29	21.95	20.23	21.89	21.23	20.91
	GIC	18.94	19.55	18.78	20.84	23.81	21.86	20.50	21.00	19.33	21.28	24.16	22.09	21.01
	Vid2Sim w/o LGM	26.87	26.59	32.57	26.53	<b>34.82</b>	26.99	24.45	31.21	<b>27.62</b>	24.83	30.01	30.33	28.57
	<b>Ours</b>	<b>28.09</b>	<b>29.67</b>	<b>32.65</b>	<b>27.97</b>	34.62	<b>29.17</b>	<b>27.67</b>	<b>33.50</b>	27.58	<b>27.46</b>	<b>30.15</b>	<b>31.49</b>	<b>30.00</b>
SSIM ↑	PAC-NeRF	0.887	0.956	0.940	0.908	0.893	0.922	0.939	0.932	0.936	0.921	0.926	0.923	0.924
	Spring-Gaus	0.867	0.941	0.941	0.903	0.912	0.919	0.948	0.917	0.937	0.920	0.921	0.920	0.920
	GIC	0.903	0.945	0.930	0.925	0.922	0.936	0.948	0.949	0.934	0.938	0.942	0.936	0.934
	Vid2Sim w/o LGM	0.931	0.959	0.973	0.937	0.955	0.942	0.944	0.973	0.954	0.936	0.952	0.963	0.952
	<b>Ours</b>	<b>0.950</b>	<b>0.972</b>	<b>0.975</b>	<b>0.948</b>	<b>0.960</b>	<b>0.957</b>	<b>0.964</b>	<b>0.980</b>	<b>0.958</b>	<b>0.954</b>	<b>0.955</b>	<b>0.971</b>	<b>0.962</b>
FoVVD ↑	PAC-NeRF	6.043	7.473	7.001	6.540	5.991	6.791	6.626	6.485	7.006	6.876	6.543	6.711	6.674
	Spring-Gaus	5.455	6.862	6.890	6.377	5.899	6.524	6.998	5.988	6.902	6.153	6.300	6.569	6.410
	GIC	6.130	6.230	6.062	6.552	5.889	6.907	6.855	6.737	6.331	6.985	7.069	6.782	6.544
	Vid2Sim w/o LGM	7.778	6.884	<b>8.792</b>	7.622	<b>9.117</b>	7.468	6.246	8.949	<b>7.681</b>	6.325	<b>8.034</b>	8.628	7.794
	<b>Ours</b>	<b>8.403</b>	<b>7.843</b>	8.783	<b>8.005</b>	8.708	<b>8.178</b>	<b>7.752</b>	<b>9.153</b>	7.617	<b>7.792</b>	7.925	<b>8.801</b>	<b>8.247</b>

Table 3. Quantitative Comparison on Future State Prediction.

	PAC-NeRF	Spring-Gaus	GIC	Vid2Sim	<b>Ours</b>
PSNR ↑	20.11	18.32	19.20	25.07	<b>25.71</b>
SSIM ↑	0.913	0.905	0.916	0.945	<b>0.948</b>
FoVVD ↑	5.948	5.443	5.702	<b>7.770</b>	7.683

gree 3 (69 parameters per convex shape). We first train 3D convexes for the undeformed space following the original 3DCS [19] and train the neural skinning network using the data-free method from [33]. We then jointly optimize  $E, \nu, \theta$  for 400 iterations using the Adam optimizer [1], with learning rates  $5 \times 10^{-3}, 1 \times 10^{-3}, 5 \times 10^{-7}$ . Simulation uses  $M = 10$  control handles as reduced DOFs. The average training time cost per scene is about 6 min on a single Nvidia RTX A6000 (Details in Sec. 5.6). Additional results for varying  $K$  and  $M$  appear in Sec. 5.5.

### 5.1. Physical System Identification

Following [7, 9, 28], we assessed our method and all baselines on physical system identification against 12 GSO test cases. As shown in Tab. 1, PhysConvex achieves the lowest error in most cases and remains competitive in the rest, validating its accuracy in recovering physical properties.

### 5.2. Dynamic Reconstruction

Our method and baselines for dynamic reconstruction were evaluated using a set of 12 GSO test cases following [7, 9, 28, 51]. For fair comparison, we use Vid2Sim’s vari-

ant that trains 3D Gaussians from scratch without initializing 3D Gaussians from pre-trained Large Multi-view Gaussian Model (LGM) [40] predictions. As shown in Tab. 2 and Fig. 4, PhysConvex achieves superior reconstruction quality and physical realism. Prior methods that optimize voxels in NeRF or ellipsoids in 3DGS often produce blurred textures or inaccurate dynamics, whereas our reduced-order, boundary-driven convex fields preserve sharp details and dynamic fidelity. Moreover, unlike grid-based MPM or spring-mass elastic dynamics, which are susceptible to numerical artifacts and oscillations in large-scale elastodynamics of complex geometries, our mesh- and grid-free reduced-space solver yields efficient, accurate dynamics.

### 5.3. Future State Prediction

We further evaluate temporal generalization following [51]. After reconstructing the first 16 frames, all methods predict the subsequent 8 frames. Average results across all test cases (Tab. 3 and Fig. 4) show that PhysConvex maintains the top accuracy, demonstrating improved physical consistency in temporal evolution.

### 5.4. Generalization Capability

We further demonstrate the generalization of our method to novel materials, forces, and boundary conditions, showing consistent performance.

**Generalization to Different Materials.** PhysConvex generalizes naturally to different material behaviors and

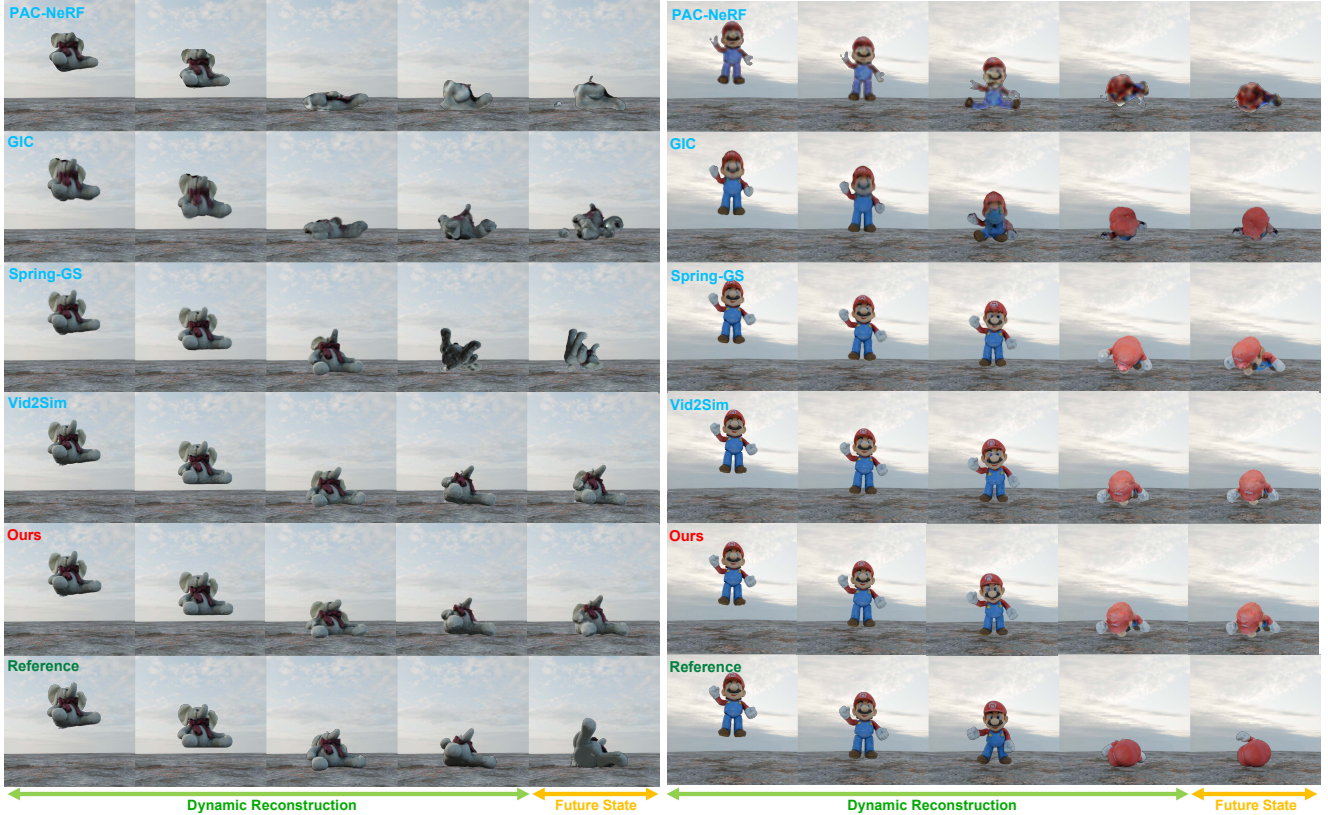


Figure 4. Comparison with baseline [7, 9, 28, 51] on dynamic reconstruction and future state prediction. Our method preserves high-quality geometry and appearance while producing physically plausible dynamics.



Figure 5. Generalization to novel materials. Elastic (stiff):  $E=10^7$ ,  $\nu=0.49$ . Elastic (soft):  $E = 8000$ ,  $\nu = 0.4$ . Plasticine:  $\tau_Y=500$ . Sand:  $\theta_f=10^\circ$ .

their constitutive models. We demonstrate this by simulating *Elastic*, *Plasticine*, and *Sand* materials following [7, 28]. As shown in Fig. 5, our method accurately captures the distinct material responses, utilizing corresponding energy densities derived for each model.

**Generalization to Complex Boundary and Force Conditions.** PhysConvex is robust to varying environmental dynamics, seamlessly integrating into dynamic scenes with novel forces and complex boundary interactions. As shown in Fig. 6, our method reliably produces stable, high-

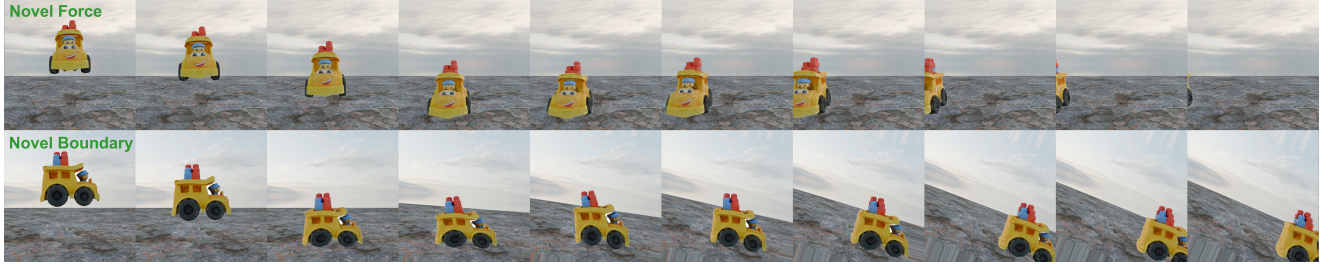


Figure 6. Generalization to novel force and complex boundary conditions. Force: A continuous external force pushing the falling object toward the left. Boundary: An object falls and is subjected to sliding motion on a continuously moving floor.

Table 4. Ablation of the Number  $K$  of Convex Points ( $M = 10$ ) ( Best , Second , Third ).

$K$	Dynamic Reconstruction			Future State Prediction			System Identification		Primitives	Training Time
	PSNR $\uparrow$	SSIM $\uparrow$	FoVVD $\uparrow$	PSNR $\uparrow$	SSIM $\uparrow$	FoVVD $\uparrow$	$\log(E)$	$\nu$	Num.	Average
K=3	24.90	0.939	6.957	19.63	0.919	6.139	0.74	0.05	11827	5min 20s
K=4	29.56	0.960	8.151	24.50	0.944	7.500	0.38	0.04	14405	5min 36s
K=5	29.88	0.961	8.235	25.09	0.946	7.688	0.36	0.04	18773	6min 5s
K=6	30.00	0.962	8.247	25.71	0.948	7.683	0.37	0.04	23681	6min 14s
K=7	30.01	0.962	8.235	24.95	0.945	7.664	0.38	0.05	29646	6min 39s
K=8	30.19	0.962	8.290	25.38	0.948	7.760	0.47	0.04	35320	7min 5s

Table 5. Ablation of the Number  $M$  of Reduced DOFs. ( Best , Second , Third )

$K$	$M$	Dynamic Reconstruction			Future State Prediction			System Identification		Primitives
		PSNR $\uparrow$	SSIM $\uparrow$	FoVVD $\uparrow$	PSNR $\uparrow$	SSIM $\uparrow$	FoVVD $\uparrow$	$\log(E)$	$\nu$	Num.
K=4	M=8	29.47	0.959	8.152	24.55	0.944	7.605	0.351	0.053	14392
	M=10	29.56	0.960	8.151	24.50	0.944	7.500	0.376	0.044	14405
	M=12	29.60	0.960	8.206	24.47	0.943	7.558	0.510	0.043	14180
K=6	M=8	29.96	0.962	8.214	25.05	0.946	7.635	0.330	0.048	23832
	M=10	30.00	0.962	8.247	25.71	0.948	7.683	0.371	0.044	23681
	M=12	29.88	0.961	8.210	24.76	0.944	7.601	0.321	0.048	23736

Table 6. Comparison on total training time and primitives number.

	PAC-NeRF	GIC	Spring-GS	Vid2Sim	Ours
Avg. Training Time	51 min	69 min	32 min	8 min	<b>6 min</b>
Primitives Num.	-	-	<b>22882</b>	31363	23681

quality reconstructions and physically consistent animations even under diverse constraints.

### 5.5. Ablation Study

Ablation studies validate two key components: the number of 3D points  $K$  per convex hull in our boundary-driven convex dynamics (Tab. 4) and the number of degrees of freedom (skinning handles)  $M$  in our reduced-order convex simulation (Tab. 5). Increasing  $K$  enhances the flexibility of convex shape representation and improves reconstruction quality, though it introduces higher computational cost and longer training time. However, gains saturate beyond  $K = 6$ . Similarly, increasing  $M$  boosts deformation expressivity but is bounded by the capacity of the neural skinning network. Despite the added complexity, our convex representation remains highly efficient, requiring fewer primitives and shorter training time than Gaussian-based methods (see Tab. 6), owing to compact convex coverage

and reduced-order simulation.

### 5.6. Efficiency Comparison

We report the average total training time and the average number of primitives required for different methods using their default settings (excluding the primitives from network-based models, PAC-NeRF and GIC). As shown in Tab. 6, our method is notably more efficient, achieving shorter training time and requiring fewer primitives compared to even highly efficient baselines like Spring-Gaus and Vid2Sim. This superior efficiency stems from the compact representation achieved by our convex primitives and the inherent performance gains of our reduced-order simulation combined with an implicit Euler solver. All tests were executed on a single NVIDIA-RTX A6000 GPU.

## 6. Conclusions and Future Work

In this work, we introduced PhysConvex, a physics-informed dynamic convex radiance field that unifies visual rendering and physical simulation. By representing deformable radiance fields with boundary-driven convex primitives and reduced-order convex dynamics, PhysCon-

Convex captures spatially adaptive, physically consistent deformation and evolving boundaries with high efficiency. Experiments show that PhysConvex achieves superior reconstruction of geometry, appearance, and dynamics, advancing the goal of physically grounded 3D dynamics. In future work, we aim to further strengthen our dynamics model by integrating geometry-aware 3D reconstruction. We also plan to develop more intuitive user interaction mechanisms, potentially enabled by recent advances in large text-to-3D generation models.

## References

- [1] Kingma DP, Ba J, Adam et al. A method for stochastic optimization. *arXiv preprint arXiv:1412.6980*, 1412(6), 2014. 6
- [2] Adam W, Bargteil, Chris Wojtan, Jessica K Hodgins, and Greg Turk. A finite element method for animating large viscoplastic flow. *ACM transactions on graphics (TOG)*, 26(3): 16–es, 2007. 2
- [3] Otman Benckroun, Jiayi Eris Zhang, Siddhartha Chaudhuri, Eitan Grinspun, Yi Zhou, and Alec Jacobson. Fast complementary dynamics via skinning eigenmodes. *ACM Transactions on Graphics*, 2023. 1, 2
- [4] J Frédéric Bonnans, J Charles Gilbert, Claude Lemaréchal, and Claudia A Sagastizábal. *Numerical optimization: theoretical and practical aspects*. Springer, 2006. 4
- [5] Sofien Bouaziz, Sebastian Martin, Tiantian Liu, Ladislav Kavan, and Mark Pauly. Projective dynamics: Fusing constraint projections for fast simulation. In *Seminal Graphics Papers: Pushing the Boundaries, Volume 2*, pages 787–797. 2023. 2
- [6] Tim Brooks, Bill Peebles, Connor Holmes, Will DePue, Yufei Guo, Li Jing, David Schnurr, Joe Taylor, Troy Luhman, Eric Luhman, et al. Video generation models as world simulators. *OpenAI Blog*, 1(8):1, 2024. 1
- [7] Junhao Cai, Yuji Yang, Weihao Yuan, Yisheng He, Zilong Dong, Liefeng Bo, Hui Cheng, and Qifeng Chen. Gic: Gaussian-informed continuum for physical property identification and simulation. *Advances in Neural Information Processing Systems*, 37:75035–75063, 2024. 1, 5, 6, 7
- [8] Yue Chang, Peter Yichen Chen, Zhecheng Wang, Maurizio M Chiamonte, Kevin Carlberg, and Eitan Grinspun. Licrom: Linear-subspace continuous reduced order modeling with neural fields. In *SIGGRAPH Asia 2023 Conference Papers*, pages 1–12, 2023. 2
- [9] Chuhan Chen, Zhiyang Dou, Chen Wang, Yiming Huang, Anjun Chen, Qiao Feng, Jiatao Gu, and Lingjie Liu. Vid2sim: Generalizable, video-based reconstruction of appearance, geometry and physics for mesh-free simulation. *IEEE Conference on Computer Vision and Pattern Recognition (CVPR)*, 2025. 1, 3, 5, 6, 7
- [10] Peter Yichen Chen, Jinxu Xiang, Dong Heon Cho, Yue Chang, GA Pershing, Henrique Teles Maia, Maurizio M Chiamonte, Kevin Carlberg, and Eitan Grinspun. Crom: Continuous reduced-order modeling of pdes using implicit neural representations. *arXiv preprint arXiv:2206.02607*, 2022. 2
- [11] Barbara Cutler, Julie Dorsey, Leonard McMillan, Matthias Müller, and Robert Jagnow. A procedural approach to authoring solid models. *ACM Transactions on Graphics (TOG)*, 21(3):302–311, 2002. 2
- [12] Boyang Deng, Kyle Genova, Soroosh Yazdani, Sofien Bouaziz, Geoffrey Hinton, and Andrea Tagliasacchi. Cvxnet: Learnable convex decomposition. In *Proceedings of the IEEE/CVF conference on computer vision and pattern recognition*, pages 31–44, 2020. 5
- [13] Mathieu Desbrun and Marie-Paule Gascuel. Smoothed particles: A new paradigm for animating highly deformable bodies. In *Computer Animation and Simulation’96: Proceedings of the Eurographics Workshop in Poitiers, France, August 31–September 1, 1996*, pages 61–76. Springer, 1996. 2
- [14] Lorenzo Diazi, Daniele Panozzo, Amir Vaxman, and Marco Attene. Constrained delaunay tetrahedrization: A robust and practical approach. *ACM Transactions on Graphics (TOG)*, 42(6):1–15, 2023. 1
- [15] Laura Downs, Anthony Francis, Nate Koenig, Brandon Kinman, Ryan Hickman, Krista Reymann, Thomas B McHugh, and Vincent Vanhoucke. Google scanned objects: A high-quality dataset of 3d scanned household items. In *2022 International Conference on Robotics and Automation (ICRA)*, pages 2553–2560. IEEE, 2022. 5
- [16] Yuanxing Duan, Fangyin Wei, Qiyu Dai, Yuhang He, Wenzheng Chen, and Baoquan Chen. 4d-rotor gaussian splatting: towards efficient novel view synthesis for dynamic scenes. In *ACM SIGGRAPH 2024 Conference Papers*, pages 1–11, 2024. 1
- [17] Chen Gao, Ayush Saraf, Johannes Kopf, and Jia-Bin Huang. Dynamic view synthesis from dynamic monocular video. In *Proceedings of the IEEE/CVF International Conference on Computer Vision*, pages 5712–5721, 2021.
- [18] Shanyan Guan, Huayu Deng, Yunbo Wang, and Xiaokang Yang. Neurofluid: Fluid dynamics grounding with particle-driven neural radiance fields. In *ICML*, 2022. 1
- [19] Jan Held, Renaud Vandeghen, Abdullah Hamdi, Adrien Deliege, Anthony Cioppa, Silvio Giancola, Andrea Vedaldi, Bernard Ghanem, and Marc Van Droogenbroeck. 3D convex splatting: Radiance field rendering with 3D smooth convexes. In *Proceedings of the IEEE/CVF Conference on Computer Vision and Pattern Recognition (CVPR)*, 2025. 2, 3, 5, 6
- [20] Alain Hore and Djemel Ziou. Image quality metrics: Psnr vs. ssim. In *2010 20th international conference on pattern recognition*, pages 2366–2369. IEEE, 2010. 5
- [21] Yuanming Hu, Luke Anderson, Tzu-Mao Li, Qi Sun, Nathan Carr, Jonathan Ragan-Kelley, and Frédo Durand. DiffTaichi: Differentiable programming for physical simulation. *arXiv preprint arXiv:1910.00935*, 2019. 2
- [22] Chenfanfu Jiang, Craig Schroeder, Joseph Teran, Alexey Stomakhin, and Andrew Selle. The material point method for simulating continuum materials. In *ACM SIGGRAPH 2016 Courses*, New York, NY, USA, 2016. Association for Computing Machinery. 2, 5
- [23] Hanxiao Jiang, Hao-Yu Hsu, Kaifeng Zhang, Hsin-Ni Yu, Shenlong Wang, and Yunzhu Li. Phystwin: Physics-

- informed reconstruction and simulation of deformable objects from videos. *ICCV*, 2025. 1, 3
- [24] Bernhard Kerbl, Georgios Kopanas, Thomas Leimkühler, and George Drettakis. 3d gaussian splatting for real-time radiance field rendering. *ACM Transactions on Graphics*, 42(4), 2023. 1
- [25] Gergely Klár, Theodore Gast, Andre Pradhana, Chuyuan Fu, Craig Schroeder, Chenfanfu Jiang, and Joseph Teran. Drucker-prager elastoplasticity for sand animation. *ACM Transactions on Graphics (TOG)*, 35(4):1–12, 2016. 2
- [26] Tassilo Kugelstadt, Jan Bender, José Antonio Fernández-Fernández, Stefan Rhys Jeske, Fabian Lössner, and Andreas Longva. Fast corotated elastic sph solids with implicit zero-energy mode control. *Proceedings of the ACM on Computer Graphics and Interactive Techniques*, 4(3):1–21, 2021. 2
- [27] Minchen Li, Zachary Ferguson, Teseo Schneider, Timothy R Langlois, Denis Zorin, Daniele Panozzo, Chenfanfu Jiang, and Danny M Kaufman. Incremental potential contact: intersection-and inversion-free, large-deformation dynamics. *ACM Trans. Graph.*, 39(4):49, 2020. 1, 4
- [28] Xuan Li, Yi-Ling Qiao, Peter Yichen Chen, Krishna Murthy Jatavallabhula, Ming Lin, Chenfanfu Jiang, and Chuang Gan. Pac-nerf: Physics augmented continuum neural radiance fields for geometry-agnostic system identification. *arXiv preprint arXiv:2303.05512*, 2023. 1, 3, 5, 6, 7
- [29] Youtian Lin, Zuozhuo Dai, Siyu Zhu, and Yao Yao. Gaussian-flow: 4d reconstruction with dynamic 3d gaussian particle. In *Proceedings of the IEEE/CVF Conference on Computer Vision and Pattern Recognition*, pages 21136–21145, 2024. 1
- [30] Jonathon Luiten, Georgios Kopanas, Bastian Leibe, and Deva Ramanan. Dynamic 3d gaussians: Tracking by persistent dynamic view synthesis. In *2024 International Conference on 3D Vision (3DV)*, pages 800–809. IEEE, 2024. 1
- [31] Rafał K Mantiuk, Gyorgy Denes, Alexandre Chapiro, Anton Kaplanyan, Gizem Rufo, Romain Bachy, Trisha Lian, and Anjul Patney. Fovvideovp: A visible difference predictor for wide field-of-view video. *ACM Transactions on Graphics (TOG)*, 40(4):1–19, 2021. 5
- [32] Ben Mildenhall, Pratul P. Srinivasan, Matthew Tancik, Jonathan T. Barron, Ravi Ramamoorthi, and Ren Ng. Nerf: Representing scenes as neural radiance fields for view synthesis. In *ECCV*, 2020. 1
- [33] Vismay Modi, Nicholar Sharp, Or Perel, David I. W. Levin, and Shinjiro Sueda. Simplicits: Mesh-free, geometry-agnostic, elastic simulation. *arXiv preprint*, 2024. 2, 4, 6
- [34] Andreas Peer, Christoph Gissler, Stefan Band, and Matthias Teschner. An implicit sph formulation for incompressible linearly elastic solids. In *Computer Graphics Forum*, pages 135–148. Wiley Online Library, 2018. 2
- [35] Albert Pumarola, Enric Corona, Gerard Pons-Moll, and Francesc Moreno-Noguer. D-nerf: Neural radiance fields for dynamic scenes. In *Proceedings of the IEEE/CVF conference on computer vision and pattern recognition*, pages 10318–10327, 2021. 1
- [36] Jiawei Ren, Liang Pan, Jiaxiang Tang, Chi Zhang, Ang Cao, Gang Zeng, and Ziwei Liu. Dreamgaussian4d: Generative 4d gaussian splatting. *arXiv preprint arXiv:2312.17142*, 2023.
- [37] Alvaro Sanchez-Gonzalez, Jonathan Godwin, Tobias Pfaff, Rex Ying, Jure Leskovec, and Peter Battaglia. Learning to simulate complex physics with graph networks. In *International conference on machine learning*, pages 8459–8468. PMLR, 2020. 1
- [38] Teseo Schneider, Jérémie Dumas, Xifeng Gao, Mario Botsch, Daniele Panozzo, and Denis Zorin. Poly-spline finite-element method. *ACM Transactions on Graphics (TOG)*, 38(3):1–16, 2019. 1, 2
- [39] Cheng Sun, Min Sun, and Hwann-Tzong Chen. Direct voxel grid optimization: Super-fast convergence for radiance fields reconstruction. In *Proceedings of the IEEE/CVF conference on computer vision and pattern recognition*, pages 5459–5469, 2022. 1
- [40] Jiaxiang Tang, Zhaoxi Chen, Xiaokang Chen, Tengfei Wang, Gang Zeng, and Ziwei Liu. Lgm: Large multi-view gaussian model for high-resolution 3d content creation. In *European Conference on Computer Vision*, pages 1–18. Springer, 2024. 5, 6
- [41] Keyu Tian, Yi Jiang, Zehuan Yuan, Bingyue Peng, and Liwei Wang. Visual autoregressive modeling: Scalable image generation via next-scale prediction. *Advances in neural information processing systems*, 37:84839–84865, 2024. 1
- [42] Zhan Tong, Yibing Song, Jue Wang, and Limin Wang. Videomae: Masked autoencoders are data-efficient learners for self-supervised video pre-training. *Advances in neural information processing systems*, 35:10078–10093, 2022. 5
- [43] Zhou Wang, Alan C Bovik, Hamid R Sheikh, and Eero P Simoncelli. Image quality assessment: from error visibility to structural similarity. *IEEE transactions on image processing*, 13(4):600–612, 2004. 5
- [44] Guanjun Wu, Taoran Yi, Jiemin Fang, Lingxi Xie, Xiaopeng Zhang, Wei Wei, Wenyu Liu, Qi Tian, and Xinggang Wang. 4d gaussian splatting for real-time dynamic scene rendering. In *Proceedings of the IEEE/CVF conference on computer vision and pattern recognition*, pages 20310–20320, 2024. 1
- [45] Tianyi Xie, Zeshun Zong, Yuxing Qiu, Xuan Li, Yutao Feng, Yin Yang, and Chenfanfu Jiang. Physgaussian: Physics-integrated 3d gaussians for generative dynamics. *arXiv preprint arXiv:2311.12198*, 2023. 1, 3
- [46] Yinghao Xu, Zifan Shi, Wang Yifan, Hansheng Chen, Ceyuan Yang, Sida Peng, Yujun Shen, and Gordon Wetstein. Grm: Large gaussian reconstruction model for efficient 3d reconstruction and generation. In *European Conference on Computer Vision*, pages 1–20. Springer, 2024. 1
- [47] Zeyu Yang, Hongye Yang, Zijie Pan, and Li Zhang. Real-time photorealistic dynamic scene representation and rendering with 4d gaussian splatting. *arXiv preprint arXiv:2310.10642*, 2023. 1
- [48] Ziyi Yang, Xinyu Gao, Wen Zhou, Shaohui Jiao, Yuqing Zhang, and Xiaogang Jin. Deformable 3d gaussians for high-fidelity monocular dynamic scene reconstruction. In *Proceedings of the IEEE/CVF conference on computer vision and pattern recognition*, pages 20331–20341, 2024. 1

- [49] Yonghao Yue, Breannan Smith, Christopher Batty, Changxi Zheng, and Eitan Grinspun. Continuum foam: A material point method for shear-dependent flows. *ACM Transactions on Graphics (TOG)*, 34(5):1–20, 2015. [2](#)
- [50] Jiayi Eris Zhang, Seungbae Bang, David I.W. Levin, and Alec Jacobson. Complementary dynamics. *ACM Transactions on Graphics*, 2020. [1](#), [2](#)
- [51] Licheng Zhong, Hong-Xing Yu, Jiajun Wu, and Yunzhu Li. Reconstruction and simulation of elastic objects with spring-mass 3d gaussians. *European Conference on Computer Vision (ECCV)*, 2024. [1](#), [2](#), [3](#), [5](#), [6](#), [7](#)